Polyphase deformation of diapiric areas in models and in the eastern Prebetics (Spain)

Eduard Roca, Maura Sans, and Hemin A. Koyi

ABSTRACT

Fingerlike bodies of evaporite rocks have been observed in many regions affected by multiple tectonic phases, such as the Atlas, the Pyrenees, or the Zagros Mountains, where they have been interpreted as fault-plane diapiric injections or collapse-related salt welds. In this article, we suggest a new interpretation of these structures as squeezed diapirs based on detailed structural and sedimentological field data of the Bicorb–Quesa diapir (eastern Prebetics) and offer five analog models, which simulate the polyphase deformation of the eastern Prebetics. In this area, diapirs formed from the Oligocene to Langhian during an extensional phase related to the opening of the Valencia Trough. These diapirs were later affected by a Serravallian contractional phase, which inverted the preexisting grabens and created new folds and thrusts. The preexisting diapirs were necked and/or squeezed, forming secondary welds with a fingerlike geometry that isolated the diapir bulbs from their source layer. Extrusion of diapiric material was also accelerated during this phase, but no new diapirs formed. Finally, the area was again affected by an extensional phase during the Tortonian, which reactivated the normal faults and created a new set of diapirs. The new diapirs formed where the overburden was thinner, that is, at the toe of the major reactivated faults. Commonly, these faults coincide with the bounding faults of the major grabens formed during the first extensional phase, and therefore, the new diapirs grow close to the location of the squeezed diapirs. The models also show that the faults created during the initial extension prevailed as the main focus for deformation during the polyphase history. Deformation in the overburden and the viscous layer was mainly accommodated along the major grabens formed during the first extensional stage. During shortening, the initial major grabens deformed as complex anticlines, and during the subsequent extensional phase, most deformation occurred by the

Manuscript received September 14, 2004; provisional acceptance February 2, 2005; revised manuscript received June 8, 2005; final acceptance July 26, 2005.

DOI:10.1306/07260504096

AUTHORS

EDUARD ROCA ~ *Grup de Geodinàmica i Anàlisi de Conques, Facultat de Geologia, Departament de Geodinàmica i Geofísica, Universitat de Barcelona, 08028 Barcelona, Spain; eduard@natura.geo.ub.es*

Eduard Roca is a professor of structural geology at the Universitat de Barcelona. He received his Ph.D. in 1992 from the Universitat de Barcelona, and then he worked for the Institut Français du Pétrole in Paris for one year until he joined the Universitat de Barcelona. His research interests include the structure of thrusts and fold belts, salt tectonics, tectonosedimentary relationships, and the tectonics of the western Mediterranean.

MAURA SANS ~ *Grup de Geodinàmica i Anàlisi de Conques, Departament de Geodinàmica i Geofísica, Universitat de Barcelona, 08028 Barcelona, Spain; present address: Cal Rovireta, Pacs del Penedès, 08729 Barcelona, Spain; sansicia@eic.ictnet.es*

Maura Sans received her M.Sc. degree in 1992 and her Ph.D. in 2000 from the Universitat de Barcelona. She worked on salt tectonics from 1990 to 2001 in extensional settings in the western Mediterranean and in contractional settings in the Pyrenees in collaboration with the potash mining companies in the Pyrenean foreland. Since 2001, she has been working as an independent consultant.

HEMIN A. KOYI ~ *Hans Ramberg Tectonic Laboratory, Department of Earth Sciences, Uppsala University, Villavägen 16, S-75236 Uppsala, Sweden; Hemin.Koyi@geo.uu.se*

Hemin Koyi is a professor in tectonics and geodynamics at the Department of Earth Sciences in Uppsala. He is a native of Kurdistan (Iraq), where he received his B.Sc. degree. He received his M.Sc. degree and his Ph.D. in tectonics and geodynamics from Uppsala University (Sweden). He was a research fellow at the Bureau of Economic Geology (Austin, Texas) between 1991 and 1993. His main research interest is the modeling of geologic processes with special emphasis on salt and thrust tectonics. He is a member of the editorial board of the *Journal of Petroleum Geology* and the consulting editor's board of the *Geological Quarterly*.

ACKNOWLEDGEMENTS

We acknowledge the support from the Generalitat de Catalunya (Grup de Recerca de Geodinàmica i Anàlisi de Conques, 2001SGR-000074) and from the Ministerio de Ciencia y Tecnologia (Proyecto CGL2004-05816-C02-01/BTE). Hemin Koyi acknowledges financial support from the Swedish Research Council Vetenskapsrådet. We thank the thorough and thoughtful reviews of Katherine A. Giles, Jim Granath, Mark G. Rowan, and AAPG editor Ernest A. Mancini, whose suggestions and comments improved this article.

collapse of these anticlines along preexisting faults, fault welds, and the flank of the squeezed diapirs. The source layer is compartmentalized, accumulating and withdrawing material in the same locations (the initial grabens and horst). As a result, the source layer is easily depleted beneath the initial horst, forming primary welds.

INTRODUCTION

The superposition of extensional and contractional deformation is a common feature in several diapiric provinces located in or close to North America, North Africa, southwest Asia, the Alpine chains of Europe, and elsewhere (Koyi 1988; Underhill, 1988; Serrano and Martínez del Olmo, 1990; Jackson and Vendeville, 1994; Letouzey et al., 1995; Roca et al., 1996; Gil, 1998; Perthuisot et al., 1999; Hafid, 2000; Alves et al., 2002; Hudec and Jackson, 2002; Rowan et al., 2003; Stovba and Stephenson, 2003; among others). However, few studies have analyzed the evolution of the inherited salt structures and their function on the kinematics and geometric features of later deformations; moreover, most of them (i.e., Vially et al., 1994; Nalpas et al., 1995; Nielsen and Vendeville, 1995; Nielsen et al., 1995; Koyi, 1998; Guglielmo et al., 2000; Fort et al., 2004) only focus on the evolution of diapirs that were overprinted by a moderate amount of shortening. Nevertheless, all these studies, mainly based not only on field examples but also on analog and numerical models, reveal the noticeable function that the preexisting diapiric structure has on the later deformation and allow recognition of a set of features that are common in the zones where preexisting diapirs are affected by later shortening (see Table 1).

In this article, we illustrate the geometric and kinematic features of structures developed in an area where diapirs, initially triggered during an extensional phase, were later affected by two different tectonic phases: first, by a contractional phase, and later, by a new extensional phase. This study is based on the analysis of field data of the diapiric eastern Prebetics province (southeastern Iberian Peninsula) and the results of scaled analog models designed to simulate a polyphase tectonic scenario. In our models, we applied similar amounts of bulk shortening and extension as the amount of initial bulk extension triggering the diapirs. This not only allowed us to obtain similar structural features to those observed in the Prebetics, but also enabled us to identify how the complete inversion was accommodated in the overburden units and diapiric structures. Comparison of model results with field data supports a new kinematic model for the development of the eastern Prebetics, which includes an initial extension followed by a later shortening and a subsequent new extensional phase. This article documents, for the first time, the modeling of shortened diapiric areas affected by later extension.

Table 1. Features of Diapiric Areas Overprinted by Shortening

	FIELD EXAMPLES	ANALOG MODELING	REFERENCES*
SYNCONTRACT. SEDIMENTS	• Broad dynamic bulge above the diapir		(1, 2, 8, 13, 25)
	• Growth strata including unconformities with high angles of onlap		(13, 29, 32, 36)
	• Significant amount of diapiric source layer components		(29, 32)
OVERBURDEN	• Inversion of preexisting normal faults		(2, 5, 6, 7, 8, 13, 21, 32, 33, 34)
	• Anticlines located where the overburden is thinnest and weakest		(7, 13, 22, 34)
	• New salt-cored detachment anticlines nucleating above the preexisting diapirs		(2, 4, 7, 9, 10, 11, 13, 15, 21, 22, 24, 30, 31, 33, 35)
	• Inversion of the preexisting grabens forming pop-ups and curvilinear (box folds) faulted anticlines		(2, 5, 11, 14, 15, 16, 17, 21, 29)
	• Deformation concentrated on the anticlines close to the extruding diapirs		(2, 5, 6, 7, 10, 15, 29, 33, 34, 36)
	• Diapirs enhanced new thrusting and the buckling of strata next to their squeezed stems		(2, 3, 5, 7, 10, 13, 16, 17, 18, 24, 32, 33, 36)
	• Extensional faults (grabens and horsts) in the hinge zone of the anticlines		(13, 16, 24, 28, 34)
DIAPIRIC ROCKS		• Most shortening was initially taken by the diapiric rocks in the stems	(1, 8, 27)
	• Elliptical diapiric planforms with the short axis parallel to the maximum shortening direction		(8, 29)
	• Diapiric rocks expelled upward in the stems		(1, 2, 4, 6, 8, 9, 10, 13, 17, 19, 20, 22, 24, 25, 27, 28, 30, 33, 36)
	• New diapirs piercing the overburden surface		(5, 12, 18, 24, 28, 30, 35)
	• Overhangs, canopies, and allochthonous lenses of diapiric rocks created from greater diapiric rock extrusion		(2, 5, 8, 24, 25, 27, 29, 33, 35, 36)
		• Continued diapir rise after source-layer depletion	(8)
	• Growth of diapirs shrinked or stopped after being thrust from their deep evaporite source		(19, 20)
		• Stress concentrated on the diapir stems	(1, 2, 11)
	• Diapirs stems closed forming salt welds		(1, 5, 8, 9, 19, 20, 22, 23, 24, 27, 29, 32, 33, 34, 36)
	• Teardrop geometry of the diapirs with the stems pinched off		(8, 9, 26, 33, 35, 36)
	• Diapir stems pinched off by thrusts detached at the source evaporite layer and developed in the diapir stems		(1, 2, 5, 7, 9, 11, 17, 18, 32, 33)
	• Regional major thrusts detached on the bottom of the source layer transporting the preexisting diapirs and modifing them only in its frontal parts		(5, 6, 11)
	• Folding of the preexisting or syncontractional overhangs		(25)

*(1) Koyi (1998); (2) Guglielmo et al. (2000); (3) Nalpas et al. (1995); (4) Jackson et al. (1994); (5) Serrano and Martínez del Olmo (1990); (6) Serrano et al. (1994); (7) Dardeau et al. (1990); (8) Nielsen et al. (1995); (9) Rowan (1995); (10) Vially et al. (1994); (11) Letouzey et al. (1995); (12) Gil (1998); (13) Davison et al. (2000); (14) Bernini et al. (2000); (15) Hafid (2000); (16) Chikhaoui et al. (2002); (17) Perthuisot et al. (1999); (18) Rasmussen et al. (1998) and Alves et al. (2002); (19) Talbot et al. (2000); (20) Stefanescu et al. (2000); (21) Scheck et al. (2003); (22) Rowan et al. (2003); (23) Giles and Lawton (1999); (24) Hudec and Jackson (2002); (25) Krzywiec et al. (2003); (26) Stille (1925); (27) Heaton et al. (1995); (28) De Ruig (1992, 1995); (29) Brinkmann et al. (1967) and Brinkmann and Lögters (1968); (30) Ala (1974); (31) Kent (1979); (32) Roca et al. (1996) and Anadón et al. (1998); (33) Martínez (1999); (34) Karakitsios (1995); (35) Mehdi et al. (2004); (36) Fort et al. (2004).

THE EASTERN PREBETICS

Geological Setting

Located in the southeastern Iberian Peninsula, the Prebetics represents the most external part of the foreland fold and thrust belt of the Betic Cordillera. It consists of a deformed wedge of para-autochthonous Jurassic to Miocene (lower Tortonian) carbonate rocks detached on Triassic evaporite and mudstone (Figures 1–3).

In its easternmost parts, the Prebetics comprises an inner fold belt in the south and a tabular frontal thrust sheet in the north, the so-called Caroig Massif, which is only marginally affected by Betic folding. The structure of both domains is complex with variably oriented folds, both reverse and normal faults, as well as diapirs composed of Triassic evaporite-mudstone (Martínez et al., 1975, 1976, 1978; García-Velez et al., 1981; De Ruig, 1992). This complex structure results from the superposition of three main Cenozoic events listed as follows (De Ruig, 1995; Roca et al., 1996):

1. An initial extension related to the opening of the Valencia Trough (Figure 1): During this extensional phase, north-northwest–south-southeast and east-northeast–west-southwest graben systems were formed and led to the triggering and development of diapirs along the graben axes. The opening of graben systems at right angles to each other indicates that, during this stage, the intermediate and maximum finite stretches (S_2 and S_1) were horizontal and extensional. Small-scale structures and paleostress analysis denote that during this stage, the least principal stress (σ_3) was orientated northwest-southeast (De Ruig, 1992), and σ_2 was oriented northeast-southwest. The age of this extensional event is latest Oligocene–early Miocene (Aquitanian) in the

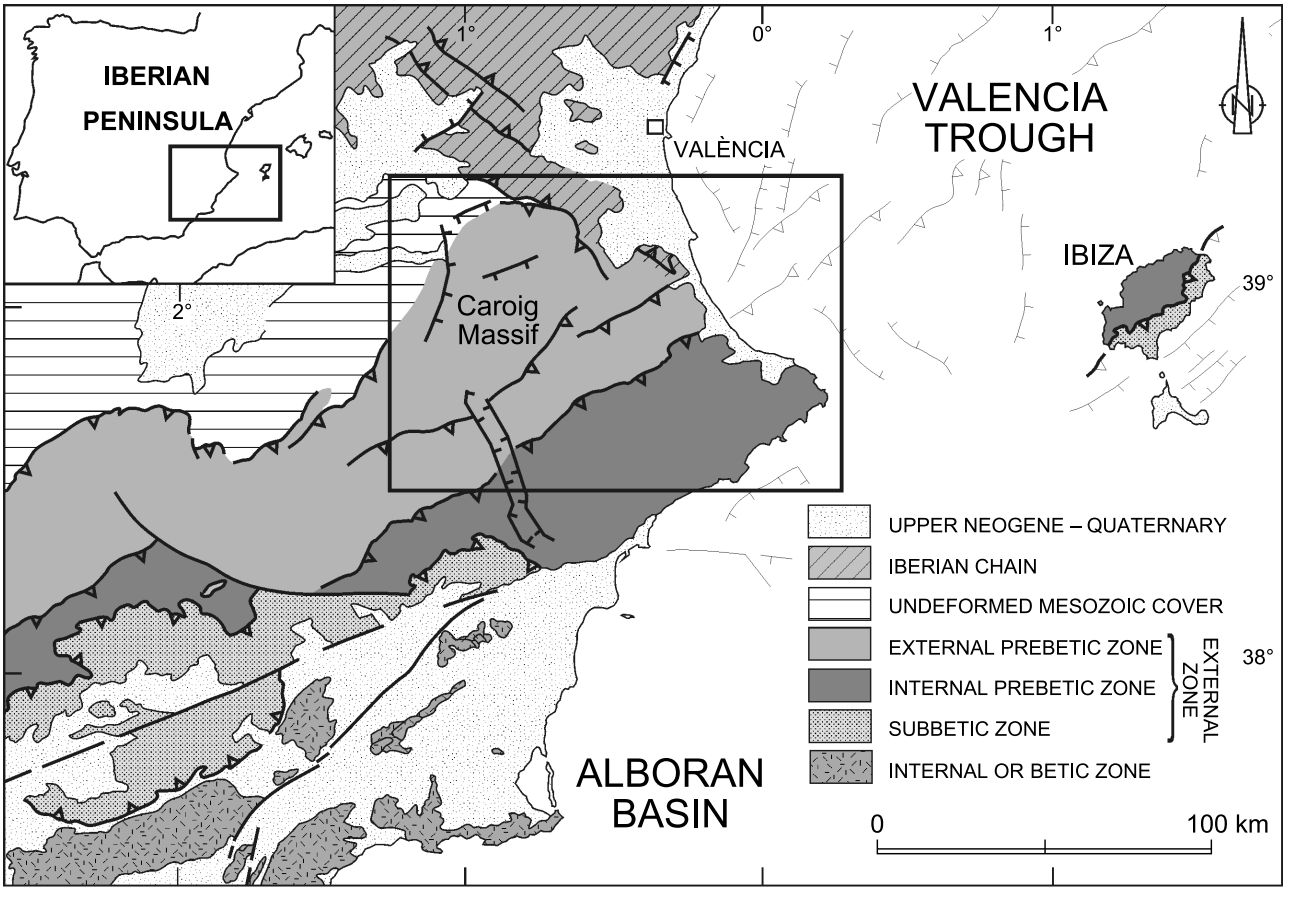

Figure 1. Tectonic map of southeast Iberia (location shown in inset). The black rectangle indicates the location of geological map shown in Figure 2. Slightly modified from Roca et al. (1996). Thick-lined faults outcrop on shore, and thin-lined faults are located offshore.

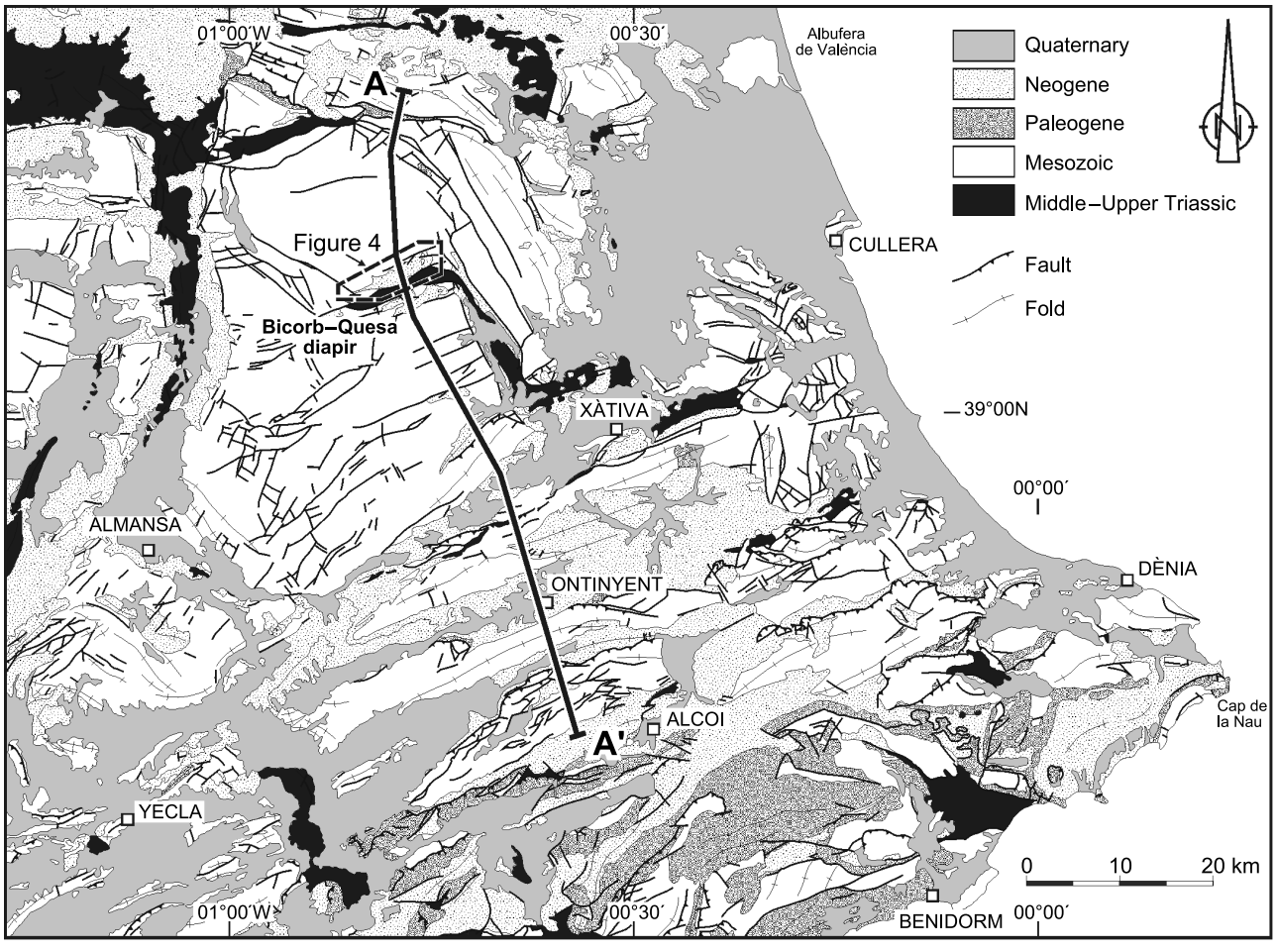

Figure 2. Simplified geological map of the eastern Prebetics with the location of cross section AA′ shown in Figure 3. Dashed inset in the Bicorb–Quesa diapir area indicates the location of geological map shown in Figure 4. Middle–Upper Triassic diapiric rocks are in black.

inner Prebetics (De Ruig, 1995) and younger in the Caroig Massif (Burdigalian to Langhian) (Santisteban et al., 1994; Roca et al., 1996).

2. A contractional to transpressional phase with a main regional stress (σ_1) direction rotating from north-northwest–south-southeast to northwest-southeast (De Ruig, 1992): This phase led to regional shortening that generated east-northeast–trending folds and thrusts and necked and/or squeezed the preexisting diapirs that had pierced the east-northeast–west-southwest grabens. This stage began during the late Aquitanian in the inner Prebetics (De Ruig et al., 1987; Ott d'Estevou et al., 1988) and propagated to the north-northwest, affecting the Caroig Massif during the Serravallian (Roca et al., 1996).
3. A final late Miocene (Tortonian) phase with radial extension (De Ruig, 1992): During this phase, normal faults were reactivated, and a new set of diapirs was initiated (Martínez, 1999).

Field data show that the predominant structures in the inner fold belt of the Prebetics are laterally continuous, east-northeast–trending, north-vergent box anticlines separated by broad synclines (Figure 3). The anticlines have very steep limbs and are cored by Middle–Upper Triassic evaporite and mudstone. The northern limbs are commonly overturned and thrusted over the adjacent synclines (García-Rodrigo, 1960; De Ruig, 1992). The crestal zone between the two box-fold hinges of these anticlines is nearly flat or broad arched, and it is commonly cut by normal faults that are subparallel and also subperpendicular to the fold axis. These normal faults form crestal grabens parallel to the fold axis, cut the Paleogene red beds, and, in some places, are blanketed by Miocene marine calcarenites tilted during the middle Miocene folding (De Ruig, 1992). Assuming that the Miocene strata have been deposited in a subhorizontal position, this indicates that these normal faults formed during the latest

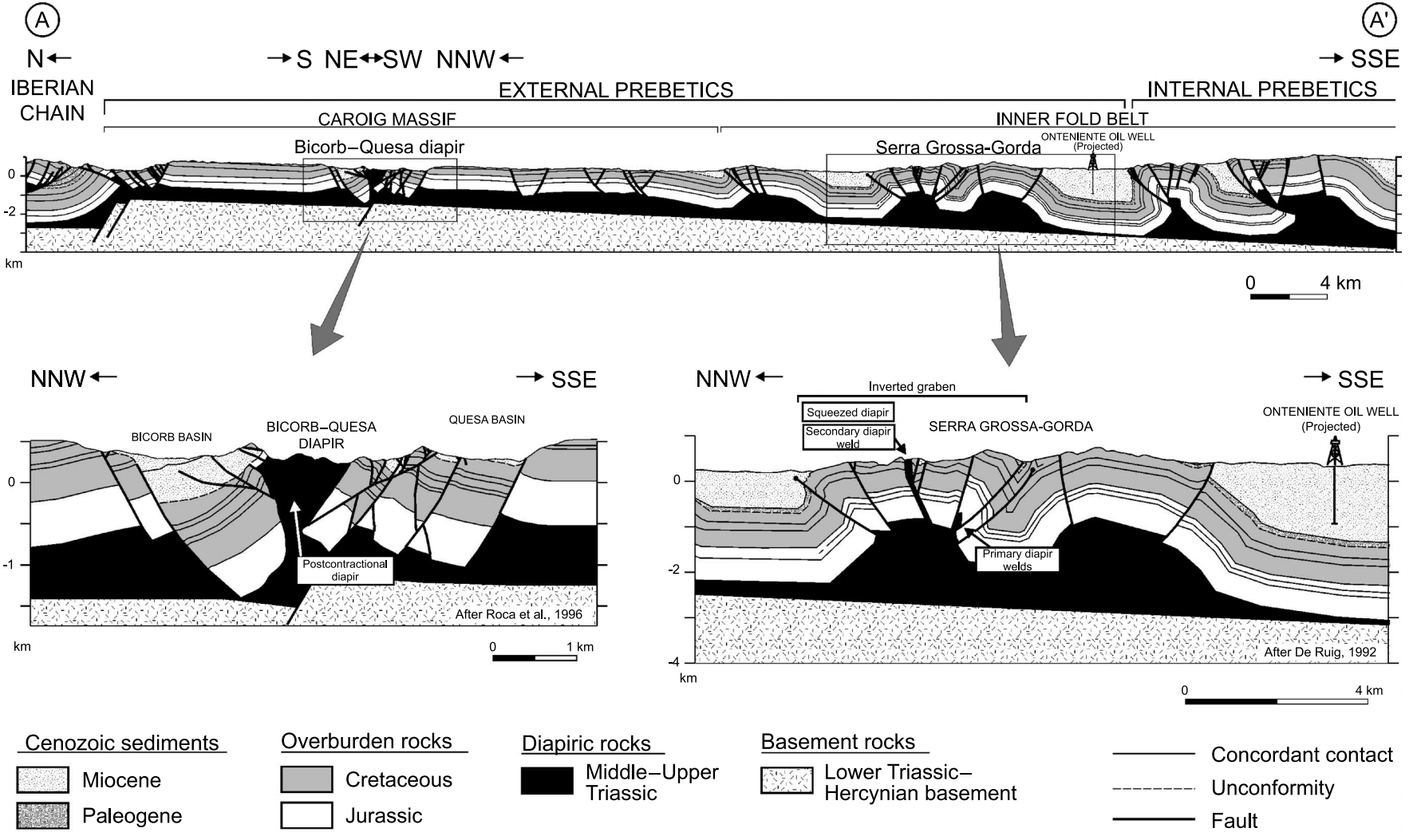

Figure 3. Balanced cross section through the eastern Prebetics showing the main features of the diapiric structures present in this area (for location, see Figure 2). Modified from an unpublished section of M. De Ruig, E. Roca, and M. Sans based on De Ruig (1992), Roca (1992), and Roca et al. (1996) data. The detailed geometry of the squeezed and postcontractional diapirs and primary and secondary welds, as well as of the overlying overburden and basin-fill rocks, are shown in the Bicorb–Quesa diapir and Serra Grossa-Gorda insets. The northern upper part of the Bicorb–Quesa diapir section is a simplification of the cross section BB′ shown in Figure 4.

Oligocene–early Miocene, and that the crestal grabens belong to extensional grabens uplifted (inverted?) during the middle Miocene compression.

The anticlines in the crestal zone, especially close to their northern limb, could be pierced by discontinuous east-northeast–west-southwest (subparallel to the fold axis) elongate and narrow (0.1–100 m; 0.3–330 ft), near-vertical planar bodies of Triassic evaporitic rocks of diapiric origin (García-Rodrigo, 1960; De Ruig, 1995; Martínez, 1999) (Figures 2, 3). The synclines, also of box-fold geometry, are filled with thick lower to middle Miocene marl and carbonate strata that locally contain olistostromes and allochthonous lenses (overhangs?) of Middle–Upper Triassic diapiric rocks (Martínez, 1999). Close to both diapir-pierced and diapir-not-pierced anticline limbs, these sediments show growth-strata geometry (De Ruig, 1992) and are affected by reverse faults, denoting that they were deposited coevally to the fold development.

To the north, this predominant fold structure disappears in the Caroig thrust sheet (Roca, 1992). This thrust sheet is composed of a subhorizontal platform of Jurassic–Cretaceous carbonates cut by two nearly orthogonal sets of normal faults that strike east-northeast–west-southwest and north-northwest–south-southeast. These normal faults bound a complex system of narrow grabens that were intruded during the Miocene by elongate diapirs of Triassic evaporite and mudstone (Moissenet, 1985) (Figures 2, 3). These diapirs rose along the axis of the graben systems that developed over Jurassic to Cretaceous carbonate overburden and were locally filled by Miocene graben fill and syndiapiric growth strata (Santisteban et al., 1989; Roca et al., 1996; Anadón et al., 1998) (Figure 4). Although they show a symmetric graben structure on both sides of the diapir, the overburden units and basin-fill sediments surrounding the east-northeast–west-southwest diapirs appear to be affected by younger reverse faults that are also pierced by the diapir (Roca et al., 1996; Anadón et al., 1998). In the Bicorb–Quesa diapir, located in the central part of the Caroig thrust sheet, the main reverse fault is a north-northwest–directed thrust that places Upper Cretaceous rocks over the lower part of the Bicorb basin fill (Figure 4). In this sector, the latter unit unconformably overlies a very thin overburden cover and even a narrow (<70-m; <230-ft), near-vertical planar body of Triassic diapiric rocks close to the fault (Figure 4). This geometry, together with the sedimentological features of the Miocene basin-fill deposits, indicates that prior to the development of the present Bicorb–Quesa diapir, an older diapir must have existed. This older diapir was squeezed and closed during the regional shortening stage (Roca et al., 1996).

Because the Caroig Massif is hardly affected by Betic folding, structural analysis of this area may assist in evaluating the prefolding structure of the more southern Prebetic domains and characterizing the geometry of the diapirs formed prior to the contractional event.

MODELING

Three dynamically scaled sand-box models (Bcp-2, Bcp-3, and Bcp-5) were designed to simulate the polyphase tectonic evolution of the outer eastern Prebetics. This includes, first, an initial extensional phase that triggered diapirism; second, a subsequent contractional phase squeezing the preexisting diapirs; and third, a second extensional phase triggering new diapirs.

The models comprise a lower viscous layer of polydimethylsiloxane (SGM-36), simulating the Triassic evaporites, and an upper tabular prekinematic layer of loose sand, simulating the Jurassic–Cretaceous carbonate cover (Figure 5). This prekinematic sand unit contained passively colored horizons of loose sand acting as strain markers. The sand and viscous layers had a similar thickness in all models (30–31 mm and 12 mm [1.18–1.22 and 0.47 in.], respectively). The thickness ratios between models and the stratigraphy of the eastern Prebetics give a geometric similarity of 1:50,000, which means that 1 km (0.62 mi) in nature is simulated by 20 mm (0.78 in.) in the models.

The rheology of the modeling materials was similar in all models. The Newtonian polydimethylsiloxane (SGM-36) has an effective viscosity at room temperature of 5×10^4 Pa s and a density of 0.987 g cm^{-3}. Assuming an effective viscosity of the Triassic evaporites to be approximately 10^{18} Pa s gives a scaling ratio of 5×10^{-14}. The loosely packed quartz sand, which has a bulk density of 1.7 g cm^{-3}, has a coefficient of internal friction of 0.73 and a cohesion of approximately 140 Pa.

The models were 30 cm (12 in.) wide and 35 cm (14 in.) long and were extended and shortened by different amounts (Table 2) from one end perpendicular to the width. Localized extension was achieved by pulling a thin metal plate, which was placed under half of the model and attached to the moving wall (Figure 5). During movement of the moving wall, the metal plate was pulled away from the fixed wall and initiated extension in both the overburden sand units and the underlying viscous source layer. During subsequent

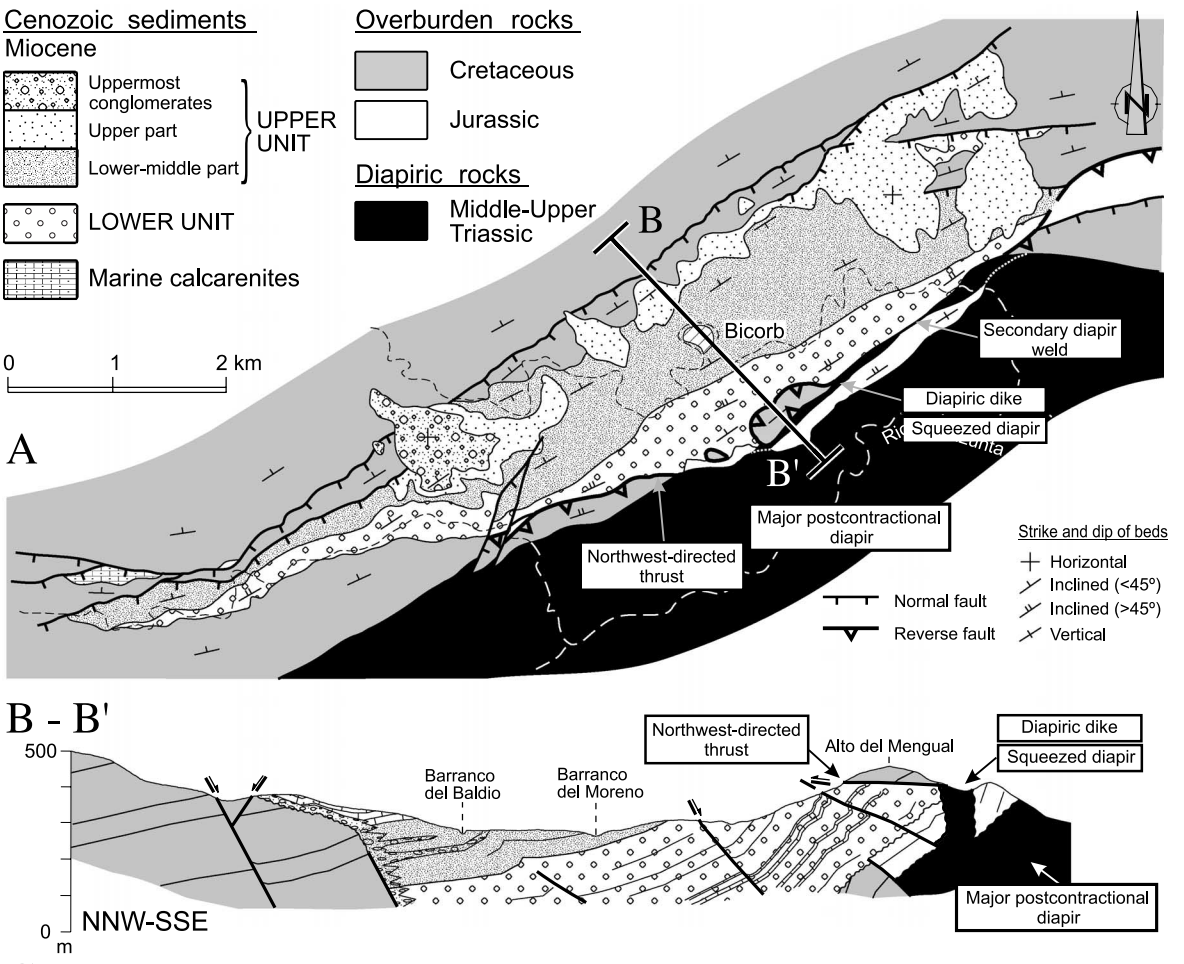
Cenozoic sediments
Miocene
Uppermost conglomerates
Upper part
Lower-middle part
UPPER UNIT
LOWER UNIT
Marine calcarenites
Overburden rocks
Cretaceous
Jurassic
Diapiric rocks
Middle-Upper Triassic
0 1 2 km
A
B
B'
Bicorb
Secondary diapir weld
Diapiric dike
Squeezed diapir
Major postcontractional diapir
Northwest-directed thrust
Strike and dip of beds
Horizontal
Inclined (<45°)
Inclined (>45°)
Vertical
Normal fault
Reverse fault
N
B - B'
500
0
m
NNW-SSE
Barranco del Baldio
Barranco del Moreno
Northwest-directed thrust
Alto del Mengual
Diapiric dike
Squeezed diapir
Major postcontractional diapir
C
Regional tectonic setting
Diapir evolution
Main sedimentological and tectosedimentary features
Records of diapir basin margin uplift
Records of diapir extrusion
Records of creation of relief near the basin
Basin-fill stratigraphy
Unit
Age
EXTENSION
COMPRESSION
EXTENSION
Diapir rise
Diapir blockage (?)
Passive stage
Active stage
Reactive stage
Diapir closure
Diapir rise
Passive stage
Attenuation of the northern main fault
Attenuation of the positive reliefs near the basin
Increase of subsidence
Lacustrine expansion
Renewal of positive reliefs near the basin
Compressive deformation along the S margin of the basin
Shallow lacustrine episodes
Attenuation of the positive reliefs near the basin
m
600
400
200
0
Upper Unit
Lower Unit
Tortonian
Serravallian
Langhian
-
Lower Miocene
Slumps
Progressive angular unconformity
Large sulfate supply
Redeposited diapir rocks
Redeposited Miocene marine fossils
Entry of coarse detritus
Alluvial mudstone
Lacustrine mudstone

compression, the wall was pushed in the opposite direction. As a result, the metal sheet moved toward the fixed wall and shortened the model. A grid with dimensions of 1.2×1.2 cm^2 (0.47×0.47 in.^{2}) was printed on the surface of the model. Marker points with specific distance were placed on either side of the fault scarps at the surface of the models to monitor the horizontal displacement and vertical growth of the structures. Shortening velocity was 1.8 or 2 cm hr^{-1} (0.7 or 0.78 in. hr^{-1}), and before applying an additional deformational event, the model was left to rest for 12 hr to allow diapirs to rise. Top-view photographs were taken at constant extension and shortening intervals during deformation. After deformation, models were covered with dry white sand to protect final topography and then soaked with water to allow cutting of longitudinal sections (parallel to the shortening and extension directions) without disturbing the model.

Model Bcp-3 underwent three deformation stages: an initial extension, a compression phase, and a second extensional phase. Model Bcp-2 underwent an initial extensional phase followed only by a compression phase, and model Bcp-5 underwent only one single extensional phase.

Two additional models (Bcp-1 and Bcp-4) were also run to test the results of such polyphase deformation with an initial extension, a subsequent compression, and a late extension. These two models were designed with different sand-box configurations, amounts of stretching, and, in the case of the Bcp-1 model, overburden thickness (Figure 5; Table 2), but their results are not significantly different than those obtained in the model Bcp-3.

MODELING RESULTS

Initial Extensional Phase

All five models underwent an initial extensional phase. Extension was initially accommodated in the overburden by layer-parallel stretching (up to 1.5–4% bulk extension) that did not form visible structures (see Bahroudi et al., 2003, for a description of penetrative extension in models). With further extension, a system of horst and grabens formed, in which undeformed blocks were bounded by planar normal faults (Figure 6). The first faults were created close to the pulling wall and above the tip of the basal slab, which can be correlated in nature to major anisotropies in the basement (i.e., older faults). During the formation of the horst and graben system, the viscous material withdrew from under the hanging wall, where the overburden was not thinned by the normal faults and the vertical overburden thickness was maximum. Migration of the viscous material promoted the rotation of the overlying overburden blocks (Figure 6) and the accumulation of viscous material under the tectonically thinned overburden areas. This subsequently resulted in the formation of reactive diapirs (Vendeville and Jackson, 1992a), which extruded along the axis of major grabens (Figure 7A).

Contractional Phase

All models, except Bcp-5, underwent a compression stage after they had been extended. Shortening was first accommodated by reducing the width of the diapirs and squeezing their stems, which forced the viscous material to extrude upward (Figure 8B). This resulted in (1) the growth of new outcropping diapirs along the preexisting reactive or active diapirs, which had not already reached the surface, from the piercing of their thin overburden; (2) the lateral expansion or growth of the outcropping diapirs from the squeezing of their shallowly buried along-strike equivalents; and (3) the development of extensive overhangs in the outcropping diapirs. Closing and emptying of the feeding stem of the preexisting diapirs created secondary, near-vertical welds isolating the diapir bulb from its source layer. These diapir bulbs have a near-vertical inverted-teardrop- or fingerlike shape and are transported by the later faults (Figure 9). No new diapirs were triggered during this contractional phase.

With increasing shortening, large complex folds formed because of the collision of several preexisting overburden blocks and the redistribution of the

Figure 4. (A) Simplified geological map of the Bicorb basin with the location of the BB′ cross section (for map location, see Figure 2). (B-B′) A more detailed cross section through the central part of the Bicorb basin showing the geometric relationships between the Miocene basin fill, the squeezed diapiric stem observed on the northern flank of the Bicorb–Quesa diapir, the later major diapir, and the faults affecting the basin fill and the overburden rocks. No vertical exaggeration. (C) Correlation chart comparing the Miocene tectonic evolution of the Bicorb–Quesa diapir with the main sedimentological and tectonostratigraphic features of the Bicorb basin fill. The synthetic stratigraphic section belongs to the central part of the Bicorb basin. Based on Roca et al. (1996) and Anadón et al. (1998).

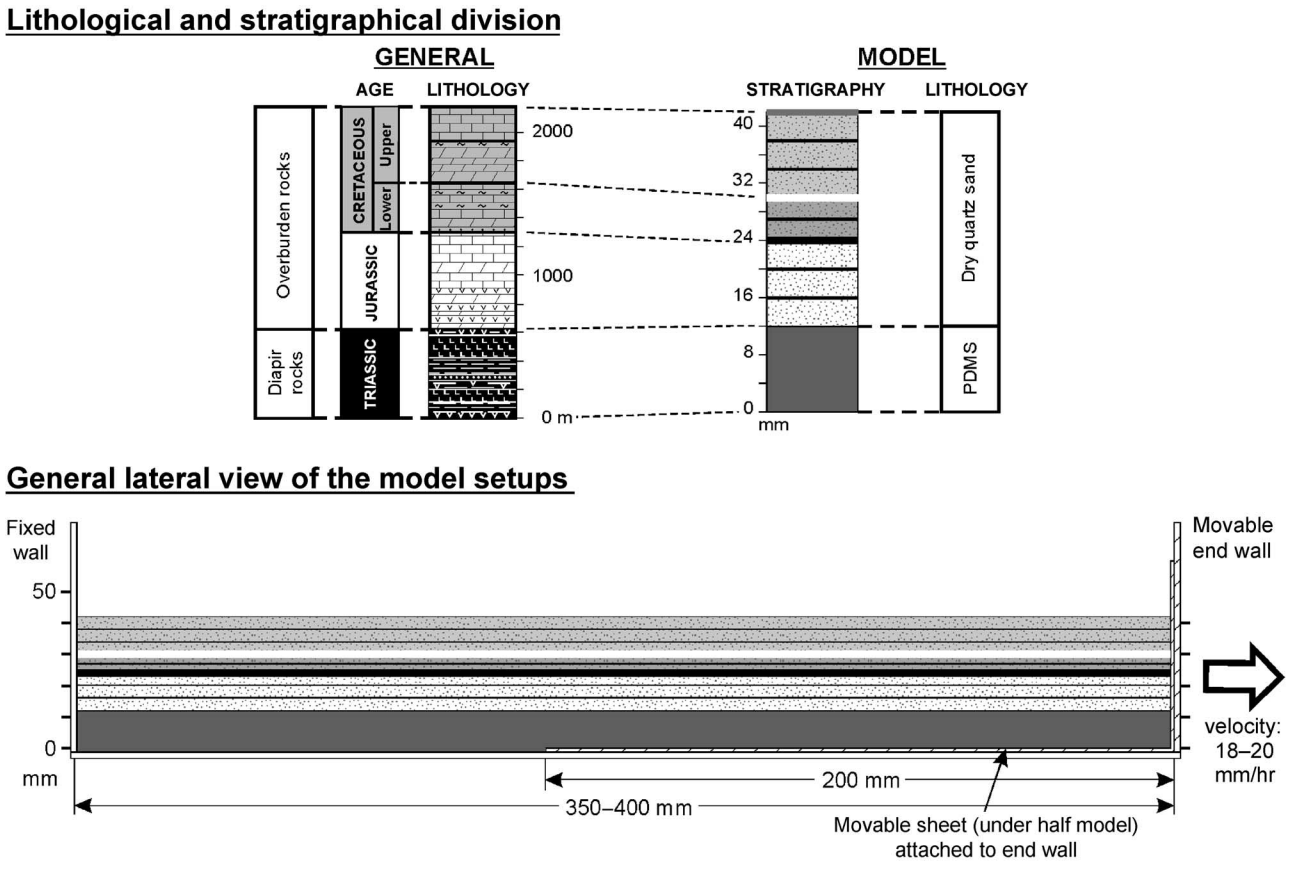

Figure 5. Schematic illustration showing the lithological and stratigraphic division of the models before deformation, as well as the general kinematic parameters used in the models. At the top, the correlation between model horizons and the regional stratigraphy of the eastern Prebetics is shown. PDMS = polydimethylsiloxane. At the middle, the general lateral view of the models Bcp-1, Bcp-2, Bcp-3, and Bcp-5 is shown. At the bottom, the top view of the box setup of the models showing major geometric differences is illustrated.

viscous material (Figure 9). The geometry and spatial distribution of these folds were strongly controlled by the preexisting structures. Synclines nucleated in the areas of preexisting horsts, whereas anticlines formed in the former graben areas where the overburden was thinner, and the viscous material was thickened and/or had pierced the overburden during the previous extension. The evolution of these major anticlines formed during this compression phase following two major stages once the diapirs were squeezed and mostly shut:

1. In the early stages of compression (Figure 8C, D), regional shortening led to the inversion of one of

Table 2. Initial Setup of Models and Kinematic Parameters*

		Model Bcp-1	Model Bcp-2	Model Bcp-3	Model Bcp-4	Model Bcp-5
Initial layer thickness	Loose sand	20 mm	30.5 mm	30 mm	31 mm	30 mm
	Polydimethylsiloxane	10 mm	12 mm	12 mm	3.7–12 mm	12 mm
Stretching and shortening velocity		18 mm hr^{-1}	18 mm hr^{-1}	18 mm hr^{-1}	20 mm hr^{-1}	20 mm hr^{-1}
Percent lengthening	First extension	17.70%	25%	28%	16%	20%
	Compression	−15%	−20.10%	−15.60%	−12.80%	
	Second extension	17%		10%	15%	

*Percent lengthening and shortening are determined considering, as initial length, the length of the model at the beginning of each applied deformation stage.

the two major faults that bounded the preexisting graben (commonly the fault dipping toward the fixed frontal wall). The resulting thrust or backthrust (depending on which fault was inverted) was detached within the viscous layer close to the overburden-viscous layer boundary and uplifted and displaced the preexisting graben and even the opposite noninverted graben margin over the overthrusted block. Reactivation of preexisting normal faults as high-angle reverse faults during this and subsequent stages also resulted in the development of minor anticlines in the adjoining footwall and hanging-wall blocks (Figure 9). These anticlines, formed when inverted normal faults splayed to shallow-dipping thrusts, were best developed in the footwalls and had the geometry of fault-propagation folds (Figure 9). They indicate that shortening was accommodated not only by inversion along preexisting normal faults, but also by the formation of thrusts nucleating at the base of the preexisting normal faults.

2. With progressive shortening, the main thrust became inactive, and shortening was accommodated by the initiation of new thrusts at the bottom of the previously overthrusted overburden block (Figure 8E). This new thrust moved in the opposite sense relative to the previous thrust and commonly did not reactivate any preexisting normal fault. The propagation of this new thrust led to folding and, later, offset of the previous active thrust and overburden units. During this stage, the inversion of preexisting major normal faults in the forelimb of the fold generated by the propagation of the new thrust could result in the development of pop-up structures (Figure 9).

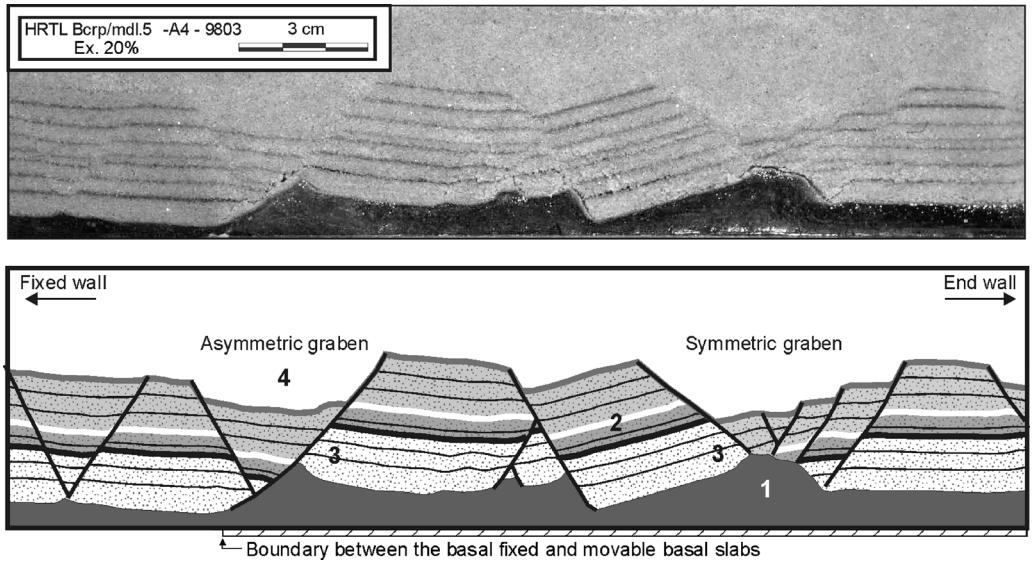

Figure 6. Photograph and line drawing of vertical sections parallel to the transport direction in model Bcp-5 after a 20% bulk lengthening showing the main geometric features of the structures that accommodate the initial extension. (1) Incipient diapir; (2) rotated overburden block; (3) uplift of the overburden at the footwall of major faults related to the rise of the ductile SGM-36 beneath the fault; (4) asymmetric graben developed above the tip of the basal sheet.

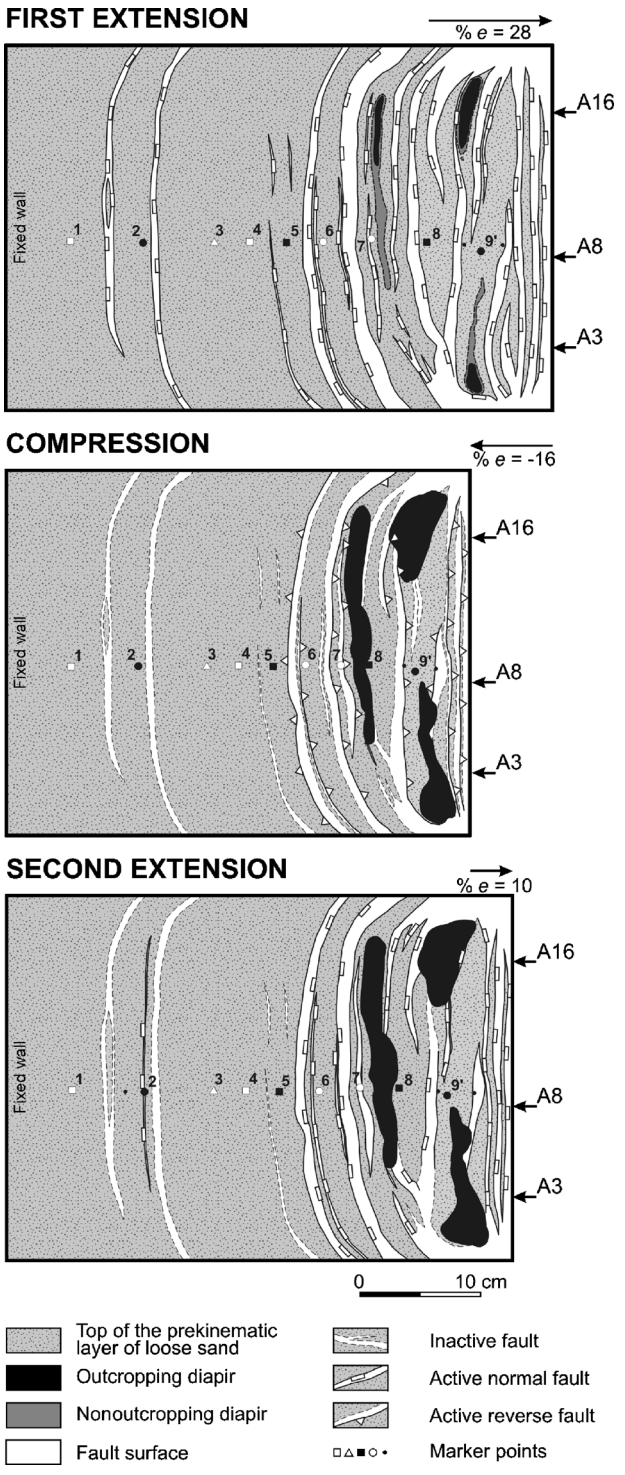

Figure 7. Line tracings of the deformation at the top of model Bcp-3 at the end of (A) the initial extensional deformation, which triggered diapirism; (B) the subsequent contractional phase, which squeezed the preexisting diapirs and inverted the older extensional faults; and (C) the second extensional phase, which led to the extensional reactivation of the preexisting faults, fault welds, and the walls of the squeezed diapirs. The small arrows labeled A16, A8, and A3 indicate the location of the three vertical parallel sections shown in Figure 10.

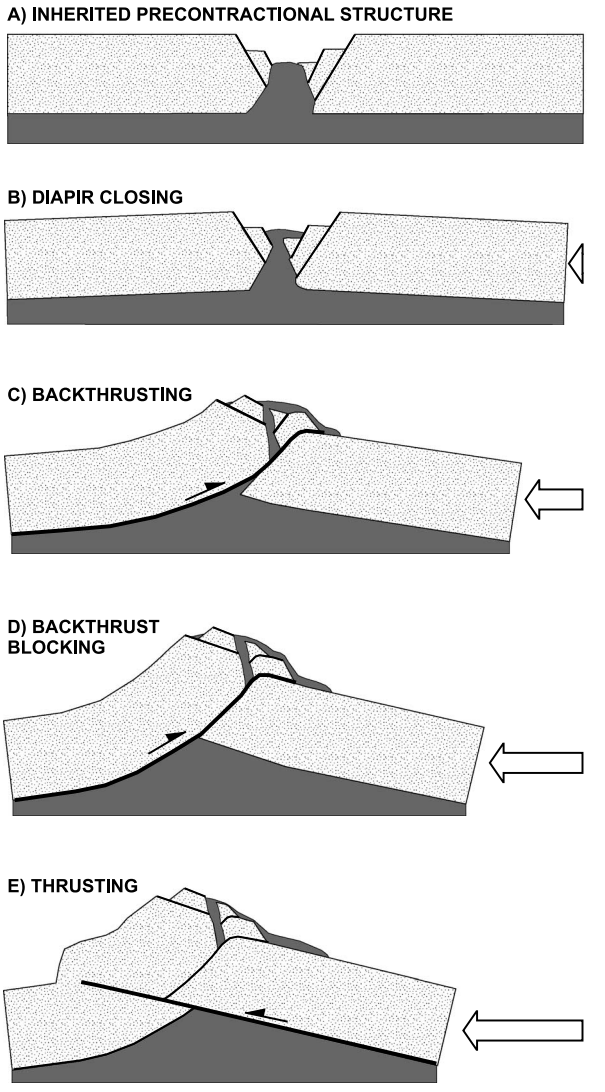

Figure 8. Cartoon showing the evolution of a preexisting graben pierced by a diapir that is subsequently shortened (based on model results).

During the contractional phase, the migration of the ductile material was accompanied by a rotation of the overburden blocks and the faults located in the major anticline limbs. This rotation produced primary salt welds beneath the synclines and, consequently, the compartmentalization of the viscous layer into isolated bodies in the cores of the major anticlines. Thrust welds of the ductile layer were also formed in the cores of the anticlines from the motion of thrust and backthrusts. In contrast to the secondary welds, these welds were subhorizontal and stratigraphically concordant with the overlying overburden materials (Figure 9). Developed after diapir closing, they separated the bottom of the secondary welds from the ductile source layer.

Second Extensional Phase

During the second extensional phase, most of the extension was accommodated in the overburden by normal reactivation of the major preexisting contractional faults and thrust welds. These contained remnants of the viscous layer and were easily reactivated as detachment levels during this second extension (Figure 10).

The coincidence of the thrusts and backthrusts with the normal faults bounding the initial grabens resulted not only in the collapse of the contractional anticlines during this second extension phase, but also in the development of a system of new grabens that were superimposed on the ones generated during the first extensional phase. In cases where the stretching resulting from this extensional phase was similar to the amount of shortening, as in our models, the most thinned overburden areas generated during the initial phase coincided with those generated in the second extensional phase.

The viscous layer was again redistributed and accumulated in areas where the ratio between the overburden and source-layer thickness was small (cores of the previously formed anticlines and grabens) and withdrew from under the footwall areas of major normal faults, which had thickened by folding and thrusting during the contractional phase. Consequently, the compartmentalization of the viscous layer initiated in the previous stages continued and formed new primary salt welds or enlarged the preexisting ones beneath the horsts (previous synclines).

Accumulation of the viscous material under the thinned overburden areas could result in the formation of new diapirs, which mainly extruded along the collapsed hinge of the anticlines close to, but at a different place from, the preexisting squeezed diapirs (Figure 10). The older, tightly squeezed diapirs behaved passively during this second extension and remained overthrusted over one of the initial overburden blocks. It should be noted that the new diapirs only grew in the areas where the ductile source layer was not isolated.

The collapse of the anticlines produced a marked inversion of the topographic relief and, therefore, of the polarity of the topographic slopes. This topographic change appears to have induced an inversion of the gravitational evaporite motion along the overhangs, from flowing away from the topographically high anticline crests during the compressional phase to flow toward the topographically low collapsing anticline crests during the superimposed extensional phase.

DISCUSSION

Role of Preexisting Structures

The comparison between the model that had undergone only extension (Bcp-5) with those that had undergone extension followed by compression (Bcp-2) and those that had undergone an initial extension followed by compression and an additional extension (Bcp-3) shows that in diapiric areas affected by polyphase thin-skinned tectonics, most of the deformation is accommodated along preexisting structures that had formed during the first stage of extension.

During compression, preexisting normal faults were inverted as high-angle reverse faults, which uplifted preexisting grabens and displaced them over undeformed horst blocks bounding the graben. The resulting contractional geometry depended on the amount of inversion and the symmetry of the preexisting grabens. In the analog models, where the grabens were relatively symmetrical, their complete inversion resulted in the development of anticlines with broad arched roofs and steep limbs. These anticlines, commonly with a pop-up crestal structure, developed from the inversion of one of the two major old normal faults bounding the graben and from newly formed backthrusts and/or the inversion of the other major old normal fault (Figure 9). The roofs (crestal zones) of the anticlines are formed by the axial part of the previous grabens, which include preexisting faults preserving its initial normal displacement.

In cases with asymmetric grabens not modeled here, we expect that compression would result in a simpler structure with transport of previous half grabens over the major thrusts developed from the inversion of normal faults bounding the half grabens.

During the second extensional phase, overburden deformation was again accommodated by normal motion along preexisting faults and, especially, along the thrust welds formed during the compression phase. The anticlines collapsed, and the resulting geometry mimicked the grabens formed during the first extensional phase. Such accommodation of deformation is shown in the relative elevation history of the initial horsts and grabens during the polyphase deformation of the models. The height of the initial horsts remains relatively constant without abrupt changes during deformation, whereas the initial grabens show a gradual and significant subsidence and uplift during the extensional and contractional phases, respectively (Figure 11).

During different tectonic phases, the viscous material migrated from areas with higher loading to areas

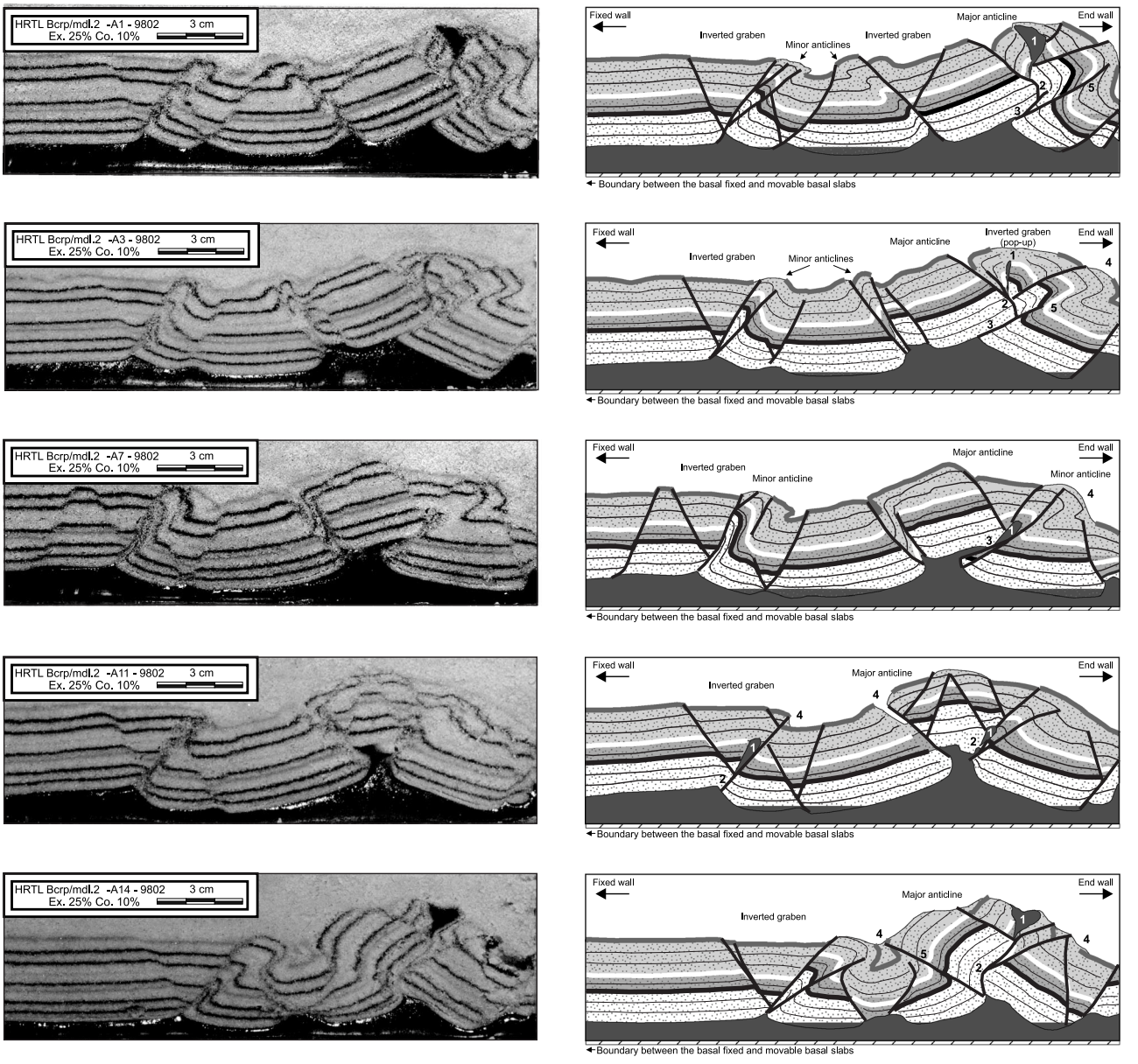

Figure 9. Photograph and line drawing of four vertical parallel sections in model Bcp-2 after an initial extension phase and a later compression phase. The sections, parallel to transport direction, show the main geometric features of the structures that accommodated the inversion. Note the significant along-axis changes (i.e., vergence) in the internal structure of the major anticline developed close to the movable end wall. (1) Squeezed diapir; (2) secondary welds; (3) thrust welds; (4) surface gravitational sand landslides; and (5) new thrust not related to the inversion of a previous normal fault.

where the overburden was thinned. If, as in our models, the amount of bulk shortening during the compression phase is equal to or slightly lower than the amount of previous extension, there will be a coincidence of the areas of withdrawal and accumulation of the viscous layer during both phases. In such cases, the compartmentalization of the viscous layer initiated during the first extensional phase and was accentuated in the later compression and extensional phases, and the viscous layer would be completely withdrawn under the synclines and horsts, forming primary welds.

Diapir Evolution

In all models, diapirs only developed when the model was extended, and the brittle overburden was significantly thinned by normal faulting. Diapirs pierced

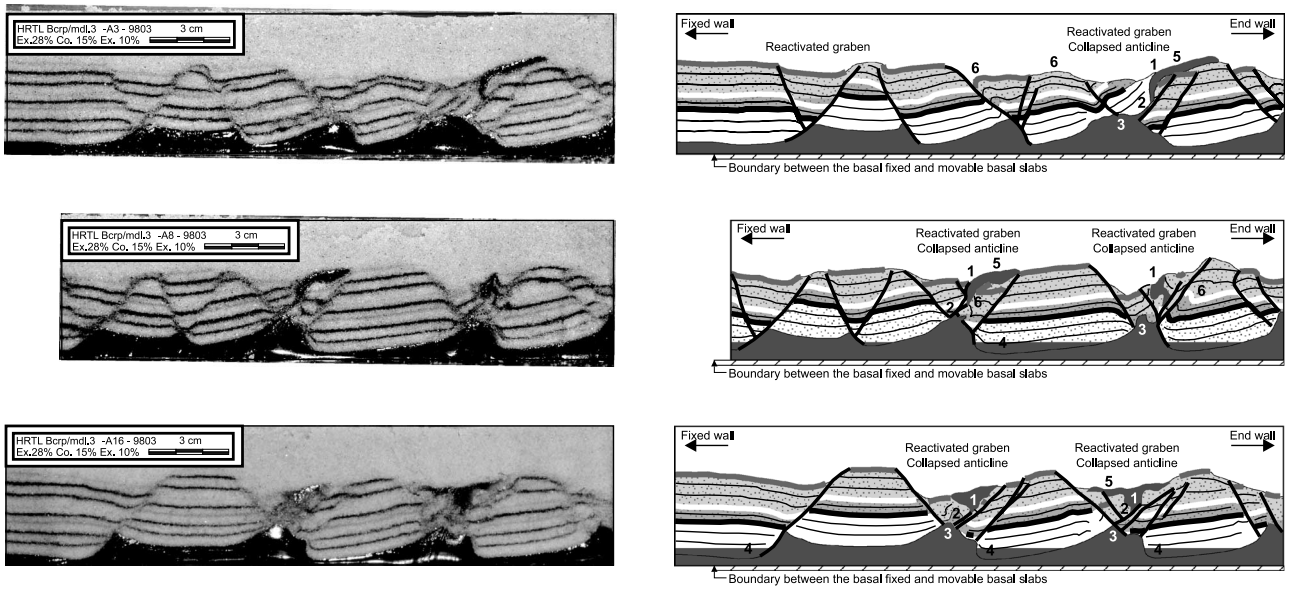

Figure 10. Photograph and line drawing of three vertical parallel sections in model Bcp-3 after an initial extension phase, a later compression phase, and an additional second extension phase (for location, see Figure 7). The sections (parallel to transport direction) show the main geometric features of the structures that accommodated the extension of a previously shortened diapiric area. Note the two generations of diapirs and the lack of significant contractional structures in the overburden. (1) Squeezed diapir (diapirs generated during the first extension); (2) extensionally reactivated secondary and thrust welds; (3) incipient diapirs triggered by the second extension; (4) developing primary weld; (5) collapsed diapir overhangs; and (6) preserved contractional structures (mainly propagation folds).

the overburden along the axis of the major grabens or along the deepest part of major half grabens. Diapir growth during regional stretching follows the evolutionary pattern defined by Vendeville and Jackson (1992a) with the reactive, active, and passive stages.

Contractional deformation did not trigger new diapirs but closed the preexisting ones, forming isolated diapiric bulbs and stems with planar, finger, or inverted-teardrop geometries. During diapir closure, the intruding viscous material was squeezed and expelled mainly upward. This resulted in (1) a sudden increase of the surface extrusion of viscous material along the preexisting diapirs, generating widespread overhangs; and (2) the formation of new extruding diapirs by the upward expelling of the viscous material along the stems of the passive diapirs, which had not already reached the surface. As described in other regions (Nielsen et al., 1995), this surge of diapiric rocks continued even after the stem of the diapir was pinched off.

After the diapir stems were closed, the ongoing compression was accommodated by the inversion of the normal faults bounding the half grabens. This resulted in the transport of the pinched diapirs over one of the graben margins, disconnecting the diapirs from their supplying layer. Placed in areas of thickened overburden, these squeezed and transported diapirs were not easily reactivated during the second extensional phase, although their flanks could be activated as normal faults.

The new diapirs formed close to the toe of the major reactivated faults, where the overburden was thinned. These faults commonly coincided with the faults bounding the major grabens formed during the first extensional phase. Consequently, new diapirs that initiated during this second extension phase were located close to or partially coincided with the position of the squeezed diapirs.

The geometry of the compressionally squeezed diapirs, in the case of planar bodies, can be similar to the hornlike diapiric cusps formed by the fall of diapirs during excessive thin-skinned extension (Vendeville and Jackson, 1992b). However, these two diapir types can be distinguished from each other by the presence of reverse faults cutting the diapiric planar body in the squeezed diapirs and the lack of surface extrusion of viscous material in the ones formed by the extensional fall of the diapirs.

Comparison with Eastern Prebetic Structure

Model results can be correlated with the structure of the eastern Prebetics and suggest a new hypothesis for the origin of vertical, narrow, planar, or fingerlike

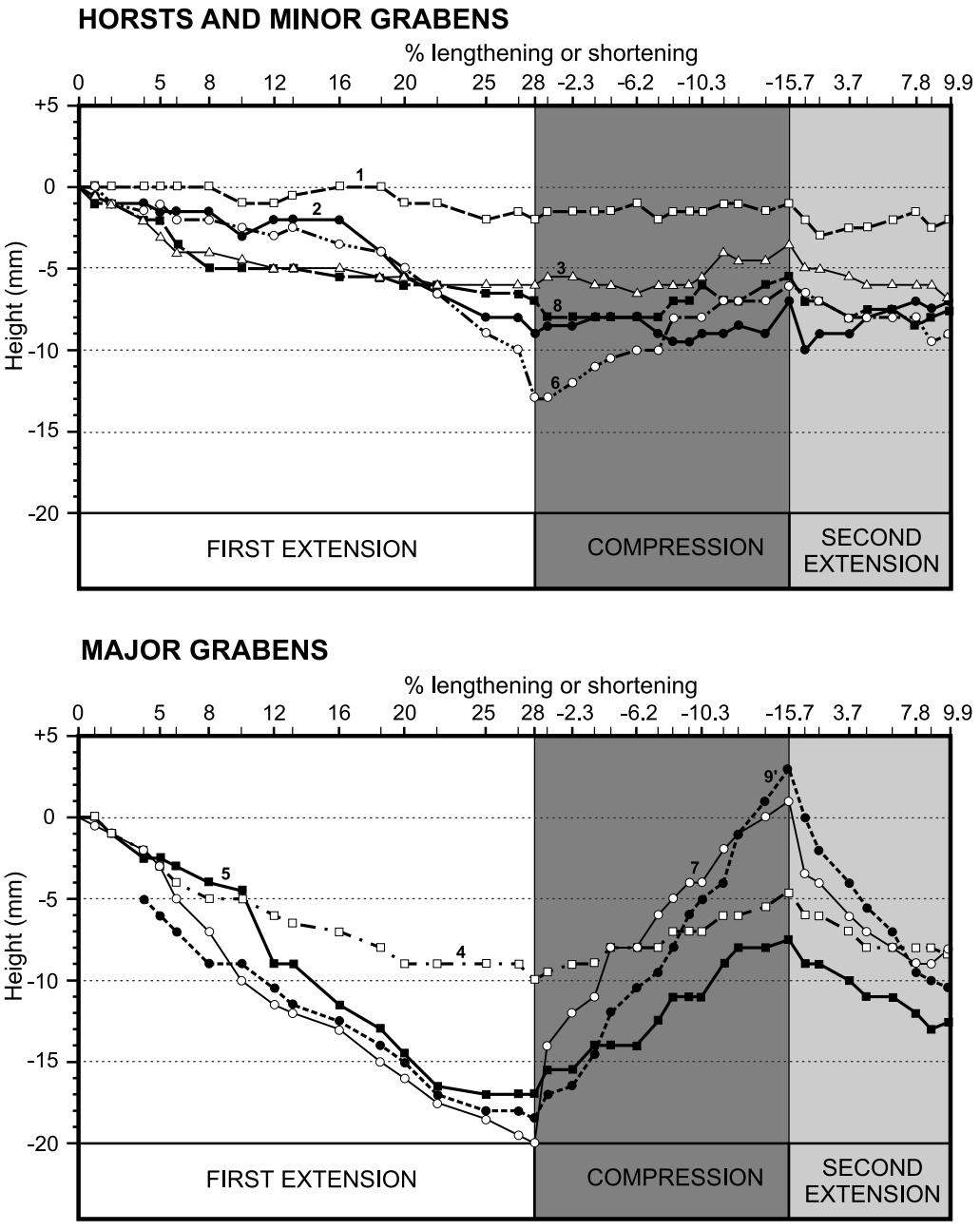

Figure 11. Diagrams showing the evolution of the relative height of initial horsts and grabens during the polyphase (extension, compression, and second extension) deformation of the model Bcp-3. Locations of marker points showing this relative height evolution are indicated in Figure 7. Percent lengthening and shortening are determined considering, as initial length, the length of the model at the beginning of each applied deformation stage.

bodies of diapiric rocks that can be observed not only in this area, but also in other diapiric regions affected by later contractional and extensional stages.

The structure of the eastern Prebetics (Figures 2–4) is consistent with moderate compressional inversion of a preexisting horst and graben system pierced by salt diapirs. Similar to the models presented here, the overburden of the inner folded Prebetics is characterized by wide and slightly deformed synclines and by narrow and complex anticlines. These complex anticlines are bounded by reverse faults and include in the hinges doubly vergent normal and reverse faults and near-vertical planar to elongate diapiric bodies (De Ruig, 1995). The diapiric bodies have been interpreted in the past as fault-plane diapiric injections emplaced along transtensional faults (García-Rodrigo, 1960; Moseley et al., 1981; De Ruig, 1992) or collapse-related salt welds (Martínez, 1999). However, their geometry and location (in the axis of the 60°-dipping conjugate fault systems) match very well with the geometries of the squeezed diapirs observed in our models. This origin as squeezed older extensional diapirs is also supported by the presence of precontractional extensional faults and precontractional sedimentary sequences, which,

unconformably overlying evaporite diapirs and containing reworked diapiric rocks (Cater, 1987; Beets and De Ruig, 1992; De Ruig, 1992), indicate that diapirs had pierced the overburden during a phase of extension before the contractional deformation (De Ruig, 1992; Martínez, 1999). According to this interpretation, the faultlike structures, including the discontinuous diapiric bodies observed in the crestal zone of the Prebetic anticlines, could be interpreted as salt welds similar to those described in the La Popa basin in Mexico (Giles and Lawton, 1999; Rowan et al., 2003).

In the northernmost eastern Prebetic areas (Caroig Massif), where a later postcontractional extensional phase has been recognized, the inferred structure and evolution of the diapirs (Roca et al., 1996) also fit very well with the results of those analog models that underwent an initial extension, triggering diapirism, a subsequent compression, and a final extension. The Bicorb–Quesa diapir, located in this area, shows the typical features of a diapir that developed during the extensional collapse of a contractional anticline, which had formed by the shortening of an older preexisting diapir. The existence of this older diapir is demonstrated by (1) the stratigraphical and structural features of the early Miocene–Langhian sediments filling the graben pierced by the diapir (Roca et al., 1996; Anadón et al., 1998); and (2) the presence of a squeezed diapiric stem (locally represented by a secondary weld) on the northern flank of the Bicorb–Quesa diapir (Figure 4). This squeezed stem belongs to the narrow, near-vertical planar body of Triassic evaporites, which, running parallel to the axis of the Bicorb–Quesa diapir, is cut by a major north-verging contractional fault (Figure 4). This fault, which also affects the older graben fill, was rotated and pierced (cut) during the growth of the Bicorb–Quesa diapir. In essence, both the Bicorb–Quesa diapir and the secondary weld record two different diapiric events separated by an intermediate stage of compression. Recording this polyphase history, the internal structure of the Bicorb–Quesa diapir reveals tight folds with vertical to overturned limbs and north-directed thrusts that are cut by the diapir.

Comparison with Other Regions and General Considerations

The geometries and evolutionary patterns observed in the analog models also facilitate the interpretation and understanding of the evolution and structure of other areas where preexisting diapirs have been affected by compression. Comparison between model results and the structure of these areas indicates that most of the recognized diapiric structures (see Table 1) have been also reproduced in our analog models. In similar conditions, this good correspondence between models and nature allows using our structural model of contractional deformation of diapirs (main features summarized in Figure 12) in understanding and/or reinterpreting structures whose diapiric significance had gone unnoticed in several regions. For example, the interpretation of planar, fingerlike, or inverted teardroplike diapiric intrusions as squeezed diapirs formed in a precontractional extension appears applicable not only to the Prebetics, but also to other contractional areas (i.e., Atlas, Pyrenees, France sub-Alpine ranges, Zagros fold-thrust belt) where such diapiric structures are relatively frequent and have been interpreted in different ways (Dardeau et al., 1990; Serrano et al., 1994; Vially et al., 1994; Bonini, 2003).

The models presented here cannot reproduce and explain all the structures observed in diapiric regions affected by later compression. This is mainly caused by differences in the initial lithological configuration, the relative amounts of bulk shortening and extension, and the obliquity between the extension and shortening directions. In addition, we have not incorporated into our models syntectonic sedimentation and/or erosion likely to affect the deformation history. In this regard, we could not reproduce the typical domes that represent the syncontractional sediments above the crest of the squeezed diapirs (Rasmussen et al., 1998; Davison et al., 2000; Krzywiec et al., 2003) or the folded geometries shown by the halokinetic sequences (Davison et al., 2000; Giles and Lawton, 2002; Rowan et al., 2003).

In cases where diapirs developed after shortening, most of the described examples relate their development to the erosion of the crestal areas of salt-cored anticlines (Sans and Koyi, 2001), to contractional generated differential loadings (Jackson and Vendeville, 1994), or to vertical amplification and strain localization along detachment folds (Bonini, 2003). Only few studies associate the growth of such diapirs to a postcompression regional extension (Underhill, 1988; Roca et al., 1996; Talbot and Alavi, 1996; Talbot et al., 2000). However, these studies commonly do not provide an accurate description of the diapirs and their surrounding overburden units. As a result, it is difficult to correlate or to compare the results of the current analog modeling with examples, apart from the Prebetics, in which contractionally squeezed diapirs

Figure 12. Cartoon showing the main structures, vertical motions, and active rotations developed during the contractional and subsequent extensional deformation of a preexisting thin-skinned horst and graben system pierced by evaporite diapirs. Note that this cartoon does not consider either erosion or sedimentation of syntectonic strata.

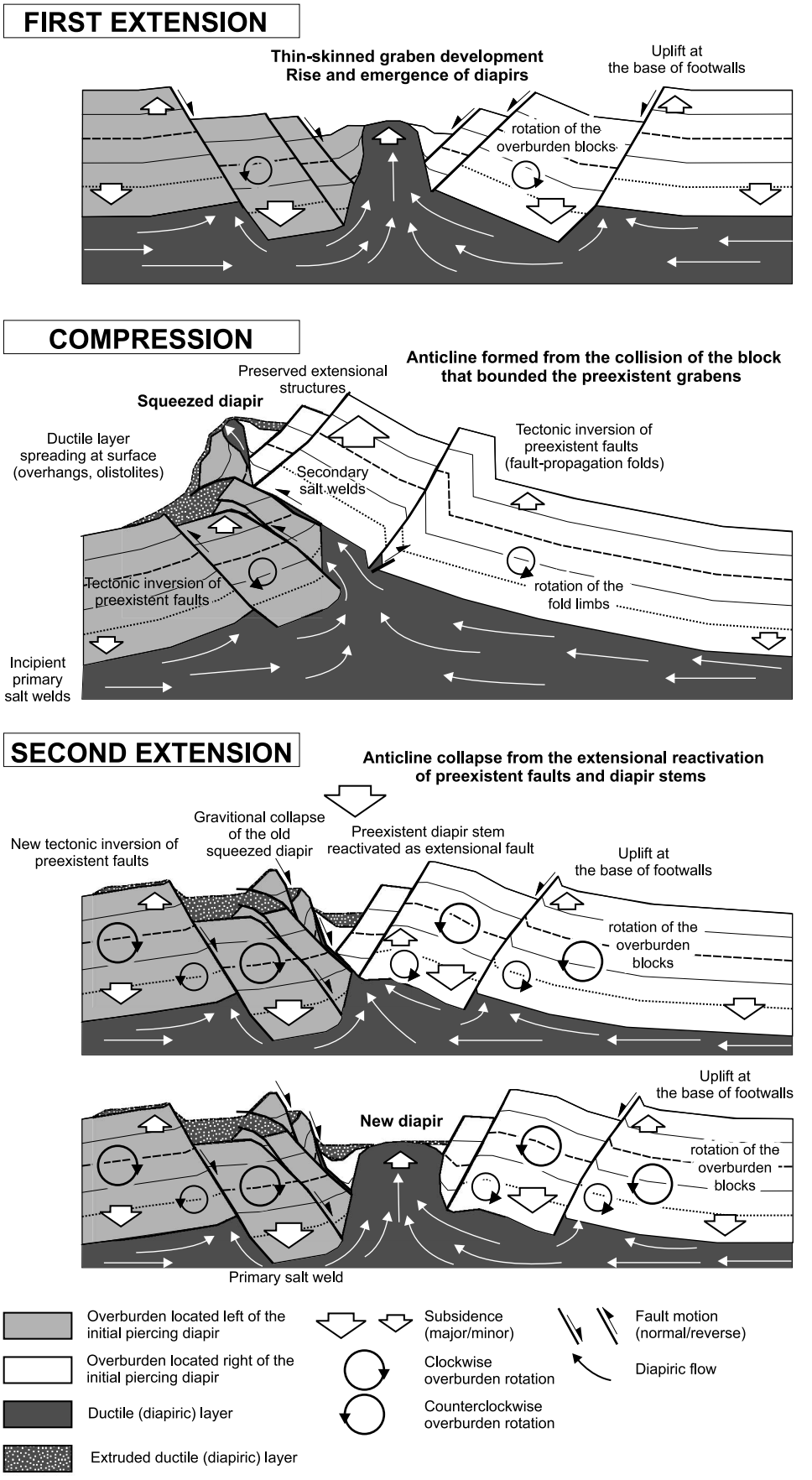

have been later affected by extension. According to our observations, diapirs formed in contractional regions affected by a later extensional phase should be located along grabens developed in the hinge of the preexisting anticlines, and they should include, in or near one of their flanks, one or more of the following: remains of squeezed diapirs, contractional structures, extensional shortcuts, and thrust welds (Figure 12). If preservation conditions are adequate and syntectonic sedimentation rates are not significantly greater than diapiric rise rates, they could also include isolated remains of the overhangs formed during the squeezing of preshortening diapirs over the horsts bounding the grabens. Identification of such structures is difficult if the stretching related to the second extension is very large; most of the structural indications will be lost or buried. Extensional reactivation of most of the preexisting faults would result in almost a complete masking of the previous structure. In such cases, the diapiric zones affected by a polyphase deformation could be confused with diapiric zones affected by only one extensional phase.

Erosion and Syndiapir Sedimentation

The analog modeling conducted in this study does not simulate erosional and depositional processes, which could be important factors in governing diapir evolution and geometry. Erosion, as well as surface collapse of evaporite-cored uplifted areas, favors diapirism because they thin the overburden units and enhance the differential loading needed to trigger diapirism (Koyi, 1998; Cotton and Koyi, 2000; Sans and Koyi, 2001; Costa and Vendeville, 2002; Sans, 2003). In addition, in wet climate areas, erosion and dissolution prevents the formation or preservation of extrusive evaporitic bodies as canopies, overhangs, or salt glaciers. Therefore, it is expected that the presence of significant erosion in a diapiric area affected later by contraction and/or extension would result in (1) an acceleration of diapir growth during extensional deformations from the erosion of the flexurally uplifted footwall blocks of major normal faults and of the overburden roof of the initiating reactive diapirs; (2) the possible formation of new diapirs across anticline crests during contractional deformation; and (3) the absence of outcropping extrusive diapiric bodies around the diapirs.

Physical and numerical modeling shows that syndiapir sedimentation prevents or renders difficult diapir development because it reduces the surface relief and strengthens and thickens the overlying cover units, thereby counteracting the tectonically induced differential loading (Vendeville and Jackson, 1992a; Jackson and Vendeville, 1994; Koyi, 1998). Models also show that the shape of the extruding diapir is controlled by sedimentation versus extension and salt supply rates (Vendeville and Jackson, 1992a, b; Koyi, 1998). In the polyphase diapiric evolution addressed here, this implies the following. (1) The observed diapir shape could be different if sedimentation processes are present during deformation. (2) Grabens may not become the locus for later contraction because significant synrift sediment thicknesses could result in the strengthening of the grabens; they may actually be stronger than the surrounding horsts. It will depend on the relative thickness of salt and overburden in each place and the function of the graben faults in weakening the overburden (M. G. Rowan, 2004, personal communication). (3) Diapir growth during extension and extrusion during compression could be held up if sedimentation rate is high. In case sedimentation could not prevent the surface extrusion of diapiric material, syntectonic sedimentation would favor preservation of allochthonous lenses, canopies, and overhangs or record this extrusion by means of the presence of chemical and detrital components in the sediments derived from the erosion of the extruding evaporitic rocks (Roca et al., 1996; Giles and Lawton, 2002).

CONCLUSIONS

Based on field data in the eastern Prebetics and results of sand-box models, thin-skinned contraction and extension of an area detached above a continuous diapiric layer display the following characteristics:

1. Diapirs only develop during extension.
2. During compression, preexisting diapirs are closed, forming secondary welds with a fingerlike geometry, which isolate diapir bulbs from their source layer. These isolated diapir bulbs show not only an inverted teardrop but also a planar or fingerlike geometry.
3. Unless the overburden thins by erosion, surface collapse, or by other processes, regional compression does not form new diapirs but accelerates extrusion of the preexisting ones.

4. Extensional deformation does not reactivate preexisting squeezed diapirs; it forms new diapirs piercing the core of the anticlines. When the preceding shortening is moderate, these new diapirs grow close to the preexisting squeezed diapirs.
5. During both contractional and extensional deformations of an area with preexisting diapirs, flow within the source layer compartmentalizes the source layer, accumulating and withdrawing it in the same locations (the initial grabens and horsts, respectively). As a result, the source layer is easily depleted beneath the initial horsts, forming primary welds.
6. Finally, in both contractional and extensional phases, deformation of the overburden and the viscous layer was mainly accommodated along the major grabens formed during the first extensional stage. During shortening, the initial major grabens deformed as complex anticlines, and during subsequent extensional phases, most deformation occurred by the collapse of these anticlines along preexisting faults, fault welds, and the flanks of the squeezed diapirs.

REFERENCES CITED

Ala, M. A., 1974, Salt diapirism in southern Iran: AAPG Bulletin, v. 58, p. 1758–1770.

Alves, T. M., R. L. Gawthorpe, D. W. Hunt, and J. H. Monteiro, 2002, Jurassic tectono-sedimentary evolution of the northern Lusitanian Basin (offshore Portugal): Marine and Petroleum Geology, v. 19, p. 727–754.

Anadón, P., F. Robles, E. Roca, R. Utrilla, and A. Vázquez, 1998, Lacustrine sedimentation in the diapir-controlled Miocene Bicorb basin, eastern Spain: Palaeogeography, Palaeoclimatology, Palaeoecology, v. 140, p. 217–243.

Bahroudi, A., H. A. Koyi, and C. J. Talbot, 2003, Effect of ductile and frictional décollements on style of extension: Journal of Structural Geology, v. 25, p. 1401–1423.

Beets, C. J., and M. J. De Ruig, 1992, $^{87}Sr/^{86}Sr$ dating of coralline algal limestones and its implications for the tectono-stratigraphic evolution of the eastern Prebetic (Spain): Sedimentary Geology, v. 78, p. 233–250.

Bernini, M., M. Boccaletti, G. Moratti, and G. Papani, 2000, Structural development of the Taza-Guercif Basin as a constraint for the Middle Atlas Shear Zone tectonic evolution: Marine and Petroleum Geology, v. 17, p. 391–408.

Bonini, M., 2003, Detachment folding, fold amplification, and diapirism in thrust wedge experiments: Tectonics, v. 22, p. 1065, doi: 10.1029/2002TC001458.

Brinkmann, R., and H. Lögters, 1968, Diapirs in western Pyrenees and foreland, Spain, *in* J. Braunstein and G. D. O'Brien, eds., Diapirism and diapirs: AAPG Memoir 8, p. 275–292.

Brinkmann, R., H. Lögters, R. Pflug, U. Von Stackelberg, P. M. Hempel, and H. D. Kind, 1967, Diapir-tektonik und stratigraphie im vorland der spanischen Westpyrenäen: Beihefte zum Geologischen Jahrbuch v. 66, 183 p.

Cater, J. M. L., 1987, Sedimentary evidence of the Neogene evolution of SE Spain: Journal of the Geological Society (London), v. 144, p. 915–932.

Chikhaoui, M., C. Jallouli, M. Moncef Turki, M. Soussi, C. Braham, and D. Zaghbib-Turki, 2002, L'affleurement triasique du Debadib-Ben Gasseur (nord-ouest de la Tunisie): Diapir enraciné à épanchements latéraux dans la mer Albienne, replissé au cours des phases de compression tertiaires: Comptes Rendus Géoscience, v. 334, p. 1129–1133.

Costa, E., and B. V. Vendeville, 2002, Experimental insights on the geometry and kinematics of fold-and-thrust belts above weak, viscous evaporitic décollement: Journal of Structural Geology, v. 24, p. 1729–1739.

Cotton, J., and H. A. Koyi, 2000, Modelling of thrust fronts above ductile and frictional décollements; examples from the Salt Range and Potwar Plateau, Pakistan: Geological Society of America Bulletin, v. 112, p. 351–363.

Dardeau, G., D. Fortwengler, P. C. Graciansky, T. Jacquin, D. Marchand, and J. Martinod, 1990, Halocinèse et jeu de blocs dans les Baronnies: Diapirs de Propiac, Montaulieu, Concorcet (Département de la Drôme, France): Bulletin des Centres de Recherche, Exploration-Production Elf-Aquitaine, v. 14, p. 111–159.

Davison, I., I. Alsop, P. Birch, C. Elders, N. Evans, H. Nicholson, P. Rorison, D. Wade, J. Woodward, and M. Young, 2000, Geometry and late-stage structural evolution of Central Graben salt diapirs, North Sea: Marine and Petroleum Geology, v. 17, p. 499–522.

De Ruig, M. J., 1992, Tectono-sedimentary evolution of the Prebetic fold belt of Alicante (SE Spain)— A study of stress fluctuations and foreland basin deformation: Ph.D. thesis, Structural Geology and Tectonics Group, Vrije Universiteit, Amsterdam, 207 p.

De Ruig, M. J., 1995, Extensional diapirism in the eastern Prebetic foldbelt, southeastern Spain, *in* M. P. A. Jackson, D. G. Roberts, and S. Snelson, eds., Salt tectonics: A global perspective: AAPG Memoir 65, p. 353–367.

De Ruig, M. J., R. M. Mier, and H. Stel, 1987, Interferences of compressional and wrenching tectonics in the Alicante region, SE-Spain: Geologie en Mijbouw, v. 66, p. 201–212.

Fort, X., J. P. Brun, and F. Chauvel, 2004, Salt tectonics on the Angolan margin, synsedimentary deformation processes: AAPG Bulletin, v. 88, p. 1523–1544.

García-Rodrigo, B., 1960, Sur la structure du Nord de la province d'Alicante (Espagne): Bulletin de la Société Géologique de France, v. 7, p. 273–277.

García-Velez, A., J. Soubrier, J. L. Goy, C. Zazo, E. Moreno, C. Martínez, I. Quintero, H. Mansilla, T. Sanz, and E. Elízaga, 1981, Mapa geológico de España E. 1:50,000. Hoja 795 Játiva: Servicio de Publicaciones del Instituto Geológico y Minero de España, Madrid, 28 p., 1 sheet.

Gil, J., 1998, Modelización geodinámica y numérica de estructuras evaporíticas (cuencas Surpirenaica y Cantábrica): Ph.D. thesis, Universitat de Barcelona, Barcelona, 199 p.

Giles, K. A., and T. F. Lawton, 1999, Attributes and evolution of an exhumed salt weld, La Popa basin, northeastern Mexico: Geology, v. 27, p. 323–326.

Giles, K. A., and T. F. Lawton, 2002, Halokinetic sequence stratigraphy adjacent to the El Papalote diapir, northeastern Mexico: AAPG Bulletin, v. 86, p. 823–840.

Guglielmo, G., B. C. Vendeville, and M. P. A. Jackson, 2000, 3-D visualization and isochore analysis of extensional diapirs overprinted bu compression: AAPG Bulletin, v. 84, p. 1095–1108.

Hafid, M., 2000, Triassic–early Liassic extensional systems and their Tertiary inversion, Essaouira Basin, Morocco: Marine and Petroleum Geology, v. 17, p. 409–429.

Heaton, R. C., M. P. A. Jackson, M. Bamahmoud, and A. S. O.

Nani, 1995, Superposed Neogene extension, contraction and salt canopy emplacement in the Yemeni Red Sea, *in* M. P. A. Jackson, D. G. Roberts, and S. Snelson, eds., Salt tectonics: A global perspective: AAPG Memoir 65, p. 333–351.

Hudec, M. R., and M. P. A. Jackson, 2002, Structural segmentation, inversion, and salt tectonics on a passive margin: Evolution of the inner Kwanza Basin, Angola: Geological Society of America Bulletin, v. 114, p. 1222–1244.

Jackson, M. P. A., and B. C. Vendeville, 1994, Regional extension as a geologic trigger for diapirism: Geological Society of America Bulletin, v. 106, p. 57–73.

Jackson, M. P. A., B. C. Vendeville, and D. D. Schultz-Ela, 1994, Structural dynamics of salt systems: Annual Review of Earth and Planetary Sciences, v. 22, p. 93–117.

Karakitsios, V., 1995, The influence of preexisting structure and halokinesis on organic matter preservation and thrust system evolution in the Ionian basin, northwest Greece: AAPG Bulletin, v. 75, p. 960–980.

Kent, P. E., 1979, The emergent Hormuz salt plugs of southern Iran: Journal of Petroleum Geology, v. 2, p. 117–144.

Koyi, H., 1988, Experimental modeling of role of gravity and lateral shortening in Zagros Mountains: AAPG Bulletin, v. 72, p. 1381–1394.

Koyi, H., 1998, The shaping of salt diapirs: Journal of Structural Geology, v. 20, p. 321–338.

Krzywiec, P., S. Burlinga, and H. Koyi, 2003, Permian–Mesozoic evolution of the Klodawa salt structure, central mid-Polish trough: Integration of seismic and mine data with analogue models (abs.): AAPG International Conference Abstracts, Barcelona 2003, CD-ROM: http://www.searchanddiscovery.com/documents/abstracts/2003barcelona/index.htm.

Letouzey, J., B. Colletta, R. Vially, and J. C. Chermette, 1995, Evolution of salt-related structures in compressional settings, *in* M. P. A. Jackson, D. G. Roberts, and S. Snelson, eds., Salt tectonics: A global perspective: AAPG Memoir 65, p. 41–60.

Martínez, W., 1999, Diapirismo de sales triásicas: Consecuencias estructurales y sedimentarias en el Prebético Oriental (Cordillera Bética, SE España), *in* E. Álvarez de Buergo, R. Merten, L. Villalobos, and J. Varela, eds., Libro homenaje a José Ramírez del Pozo: Asociación de Geólogos y Geofísicos Españoles del Petróleo, p. 175–187.

Martínez, W., M. Benzaquen, I. Cabañas, M. A. Uralde, E. Perconig, and I. Quintero, 1975, Mapa geológico de España E. 1:50,000. Hoja 820 Onteniente: Servicio de Publicaciones del Instituto Geológico y Minero de España, Madrid, 49 p., 1 sheet.

Martínez, W., M. Benzaquen, I. Cabañas, M. A. Uralde, L. Grambast, L. Granados, R. Shroeder, E. Perconig, and I. Quintero, 1976, Mapa geológico de España E. 1:50,000. Hoja 794 Canals: Servicio de Publicaciones del Instituto Geológico y Minero de España, Madrid, 37 p., 1 sheet.

Martínez, W., I. Colodrón, A. Núñez, I. Cabañas, M. A. Uralde, I. Quintero, C. Martínez, L. Granados, G. Leret, V. Ruíz, and J. Suárez, 1978, Mapa geológico de España E. 1:50,000. Hoja 846 Castalla: Servicio de Publicaciones del Instituto Geológico y Minero de España, Madrid, 32 p., 1 sheet.

Mehdi, K., R. Griboulard, and C. Bobier, 2004, Rôle de l'halocinèse dans l'évolution du bassin d'Essaouira (Sud-Ouest marocain): Comptes Rendus Géoscience, v. 336, p. 587–595.

Moissenet, E., 1985, Les dépressions tarditectoniques des Chaînes Ibériques méridionales: Distension, diapirisme et dépots neogènes associés: Comptes Rendus de l'Académie des Sciences, Paris, v. 300, p. 523–528.

Moseley, F., J. C. Cuttell, E. W. Lange, D. Stevens, and J. R. Warbrick, 1981, Alpine tectonics and diapiric structures in the pre-Betic zone of southeast Spain: Journal of Structural Geology, v. 3, p. 237–251.

Nalpas, T., S. Le Douaran, J. P. Brun, P. Unternehr, and J. P. Richert, 1995, Inversion of the Broad Fourteens Basin (offshore Netherlands), a small-scale model investigation: Sedimentary Geology, v. 95, p. 237–250.

Nielsen, K. T., and B. V. Vendeville, 1995, Episodic growth of salt diapirs driven by horizontal shortening: Gulf Coast Section SEPM Foundation 16th Annual Research Conference, Salt, Sediment and Hydrocarbons, p. 285–295.

Nielsen, K. T., B. V. Vendeville, and J. T. Johansen, 1995, Influence of regional tectonics on halokinesis in the Nordkapp Basin, Barents Sea, *in* M. P. A. Jackson, D. G. Roberts, and S. Snelson, eds., Salt tectonics: A global perspective: AAPG Memoir 65, p. 413–436.

Ott d'Estevou, Ph., Ch. Montenat, F. Ladure, and L. Pierson d'Autrey, 1988, Évolution tectono-sédimentaire du domaine prébétique oriental (Espagne) au Miocène: Comptes Rendus de l'Académie des Sciences, Paris, v. 307, p. 789–796.

Perthuisot, V., A. Bouzenoune, N. Hatira, B. Henry, E. Laatar, A. Mansouri, H. Rouvier, A. Smati, and J. Thibieroz, 1999, Les diapirs du Maghreb oriental: Part des déformations alpines et des structures initiales crétacées et éocènes dans les formes actuelles: Bulletin de la Société Géologique de France, v. 170, p. 57–65.

Rasmussen, E. S., S. Lomholt, C. Andersen, and O. V. Vejbaek, 1998, Aspects of the structural evolution of the Lusitanian Basin in Portugal and the shelf and slope area offshore Portugal: Tectonophysics, v. 300, p. 199–225.

Roca, E., 1992, L'estructura de la conca Catalano-balear: Paper de la compressió i de la distensió a la seva gènesi: Ph.D. thesis, University of Barcelona, Barcelona, 330 p.

Roca, E., P. Anadón, R. Utrilla, and A. Vázquez, 1996, Rise, closure and reactivation of the Bicorb–Quesa diapir, eastern Prebetics, Spain: Journal of the Geological Society (London), v. 153, p. 311–321.

Rowan, M. G., 1995, Structural styles and evolution of allochthonous salt, central Louisiana outer shelf and upper slope, *in* M. P. A. Jackson, D. G. Roberts, and S. Snelson, eds., Salt tectonics: A global perspective: AAPG Memoir 65, p. 199–228.

Rowan, M. G., T. F. Lawton, K. A. Giles, and R. A. Ratliff, 2003, Near-salt deformation in La Popa basin, Mexico, and the northern Gulf of Mexico: A general model for passive diapirism: AAPG Bulletin, v. 87, p. 733–756.

Sans, M., 2003, From thrust tectonics to diapirism. The role of evaporites in the kinematic evolution of the eastern South Pyrenean front: Geologica Acta, v. 1, p. 239–259.

Sans, M., and H. A. Koyi, 2001, Modeling the role of erosion in diapir development in contractional settings, *in* H. A. Koyi and N. S. Mancktelow, eds., Tectonic modeling: A volume in honor of Hans Ramberg: Geological Society of America Memoir 193, p. 111–122.

Santisteban, C., F. J. Ruiz-Sánchez, and D. Bello, 1989, Los depósitos lacustres del Terciario de Bicorp (Valencia): Acta Geologica Hispanica, v. 24, p. 299–307.

Santisteban, C., F. J. Ruiz-Sánchez, and J. I. Lacomba, 1994, Estratigrafía, edad y evolución de los depósitos terciarios de la cuenca de antepaís de Quesa-Bicorp (Valencia). Comunicaciones: II Congreso Español del Terciario, Jaca, p. 209–212.

Scheck, M., U. Bayer, and B. Lewerenz, 2003, Salt movements in the northeast German basin and its relation to major post-Permian tectonic phases— Results from 3D structural modelling, backstripping and reflection seismic data: Tectonophysics, v. 361, p. 277–299.

Serrano, A., and W. Martínez del Olmo, 1990, Tectónica salina en el Dominio Cántabro-Navarro: Evolución, edad y origen de las

estructuras salinas, *in* F. Ortí and J. M. Salvany, eds., Formaciones evaporíticas de la Cuenca del Ebro y cadenas periféricas, y de la zona de Levante: Barcelona, Universitat de Barcelona, p. 39–53.

Serrano, A., P. P. Hernaiz, J. Malagón, and C. Rodríguez Cañas, 1994, Tectónica distensiva y halocinesis en el margen SO de la cuenca Vasco-Cantábrica: Geogaceta, v. 15, p. 131–134.

Stefanescu, M., O. Dicea, and G. Tari, 2000, Influence of extension and compression on salt diapirism in its type area, east Carpathians bend area, Romania, *in* B. C. Vendeville, Y. Mart, and J. L. Vigneressa, eds., Salt, shale and igneous diapirs in and around Europe: Geological Society (London) Special Publication 174, p. 131–147.

Stille, H., 1925, The upthrust of the salt masses of Germany: AAPG Bulletin, v. 9, p. 417–441.

Stovba, S. M., and R. A. Stephenson, 2003, Style and timing of salt tectonics in the Dniepr-Donets Basin (Ukraine): Implications for triggering and driving mechanisms of salt movement in sedimentary basins: Marine and Petroleum Geology, v. 19, p. 1169–1189.

Talbot, C. J., and M. Alavi, 1996, The past of a future syntaxis across the Zagros, *in* G. I. Alsop, D. J. Blundell, and I. Davison, eds., Salt tectonics: Geological Society (London) Special Publication 100, p. 89–109.

Talbot, C. J., S. Medvedev, M. Alavi, H. Shahrivar, and E. Heidari, 2000, Salt extrusion at Kuh-e-Jahani, Iran, from June 1994 to November 1997, *in* B. C. Vendeville, Y. Mart, and J. L. Vigneressa, eds., Salt, shale and igneous diapirs in and around Europe: Geological Society (London) Special Publication 174, p. 93–110.

Underhill, J. R., 1988, Triassic evaporites and Plio-Quaternary diapirism in western Greece: Journal of the Geological Society (London), v. 145, p. 269–282.

Vendeville, B. C., and M. P. A. Jackson, 1992a, The rise of diapirs during thin-skinned extension: Marine and Petroleum Geology, v. 9, p. 331–353.

Vendeville, B. C., and M. P. A. Jackson, 1992b, The fall of diapirs during thin-skinned extension: Marine and Petroleum Geology, v. 9, p. 354–371.

Vially, R., J. Letouzey, F. Bénard, N. Haddadi, G. Desforges, H. Askri, and A. Boudjema, 1994, Basin inversion along the North African margin, the Saharan Atlas (Algeria), *in* J. Roure, ed., Peri-Tethyan platforms: Paris, Technip, p. 79–118.